Carbohydrate Research 344 (2009) 1575–1581

Contents lists available at ScienceDirect

Carbohydrate Research

journal homepage: www.elsevier.com/locate/carres

Metadynamics modelling of the solvent effect on primary hydroxyl rotamer equilibria in hexopyranosides

Vojtěch Spiwok [a,b,*], Igor Tvaroška [b]

[a] Department of Biochemistry and Microbiology, Institute of Chemical Technology in Prague, Technická 3, 166 28 Prague 6, Czech Republic
[b] Department of Structure and Function of Saccharides, Institute of Chemistry, Centre for Glycomics, Slovak Academy of Sciences, Dúbravska cesta 9, 84538 Bratislava, Slovakia

ARTICLE INFO

Article history:
Received 25 February 2009
Received in revised form 29 April 2009
Accepted 13 May 2009
Available online 23 May 2009

Dedicated to Professor Dr. Hans Kamerling on the occasion of his 65th birthday

Keywords:
Saccharide conformation
Gauche effect
C-5–C-6 rotamers
Free energy
Metadynamics
GLYCAM

ABSTRACT

Accurate modelling of rotamer equilibria for the primary hydroxyl groups of monosaccharides continues to be a great challenge of computational glycochemistry. The metadynamics technique was applied to study the conformational free energy surfaces of methyl α-D-glucopyranoside and methyl α-D-galactopyranoside, employing the GLYCAM06 force field. For both molecules, seven to eight conformational free-energy minima, differing in the ω (O-5–C-5–C-6–O-6) and χ (C-3–C-4–O-4–HO-4) dihedral angles, were identified in vacuum or in a water environment. The calculated rotamer equilibrium of the primary hydroxyl group is significantly different in vacuum than in water. The major effect of a water environment is the destabilisation of a hydrogen bond between O-4–HO-4 and O-6–HO-6 groups. It was possible to calculate the free-energy differences of individual rotamers with an accuracy of better than 2 kJ/mol. The calculated *gg*, *gt* and *tg* rotamer populations in water are in close agreement with experimental measurements, and therefore support the theoretical background of metadynamics.

1. Introduction

Carbohydrate recognition by proteins and other molecular partners is essential to many biological processes such as interactions of immune system components, cell–cell adhesions, metastasis and pathogen entry into a cell. Numerous carbohydrates and carbohydrate mimics are currently being developed to therapeutically intervene in these processes. Analogously, artificial carbohydrate-recognising systems offer great potential as carbohydrate sensors or therapeutics. Moreover, cleavage of highly abundant carbohydrates is nowadays widely studied as a potential source of future fuels. An understanding of carbohydrate conformation and dynamics is essential for future development of carbohydrate-based biotechnologies.

An important feature of oligosaccharides is that they usually do not contain secondary structure elements typical for most proteins, nucleic acids or polysaccharides with repeating sequences. Instead, oligosaccharides are typically present in solution in multi-conformational families. This complicates experimental determination of their three-dimensional structures using X-ray crystallography and NMR spectroscopy, yet, on the other hand, it provides a great opportunity for the application of molecular modelling techniques. Numerous successful applications of molecular dynamics simulation for modelling carbohydrate conformation have been presented in the last several decades.[1]

The major disadvantage of molecular dynamics simulation is that this method is relatively computationally expensive. In principle, it is possible to calculate conformational equilibria from probabilities of individual conformations during a long molecular dynamics simulation. However, time scales accessible by molecular dynamics simulations are often not long enough to allow the modelled carbohydrate to explore all populated conformations. Transitions between these families are often too rare to be observed in a reasonable time scale. Even if the carbohydrate can change between conformational families, their populations usually cannot be measured within an acceptable degree of accuracy. Numerous molecular modelling techniques have been developed to improve sampling of molecular dynamics simulation by use of an artificial degree of freedom (e.g., free-energy perturbation), bias potential or force (e.g., umbrella sampling or metadynamics), parallel tempering or other principles. Recently introduced metadynamics is a rapidly developing technique that improves sampling and allows for the calculation of a low-dimensional free-energy surface.[2,3]

The first step of the application of metadynamics is a selection of few (in this study two) collective variables. These are parameters

* Corresponding author. Tel.: +420 220 44 30 28; fax: +420 220 44 51 67.
E-mail addresses: chemspiw@savba.sk, spiwokv@vscht.cz (V. Spiwok), chemitsa@savba.sk (I. Tvaroška).

0008-6215/$ - see front matter © 2009 Elsevier Ltd. All rights reserved.
doi:10.1016/j.carres.2009.05.019

describing the most important slow degrees of freedom in the studied system. The repertoire of collective variables applied in metadynamics includes distances, angles, coordination numbers, collective motions, crystallographic parameters and others (see Ref. 3). Then the system is simulated by a standard molecular dynamics simulation with an additional history-dependent bias potential. The bias potential is defined as a sum of Gaussian hills located in the space of collective variables:

$$V_{\text{bias}} = \sum_{t'<t} \prod_{j} w_{t'} \exp\left[\frac{-(s_j(x) - s_j^{t'})^2}{2\delta s_j^2}\right] \quad (1)$$

where w is height of a hill and δs are its widths. During the simulation, every G-th step (in this study $G = 1000$ steps, 1 ps) a Gaussian hill is added to the standard molecular mechanical potential. These hills cumulate until they flood certain free-energy minimum and allow the system to overcome the free-energy barrier and to explore much wider range of configurations. Moreover, a final bias potential approximates a low-dimensional free-energy surface of the studied system, that is, for certain values of collective variables it is possible to calculate equilibrium probability of corresponding states (e.g., conformations). Metadynamics has been successfully applied in numerous fields, such as the modelling of conformational equilibria,[4] chemical reactivity[5] or phase transitions.[6]

In spite of recent progress in the modelling of saccharides, a simple description of the conformational equilibria of hydroxyl and primary hydroxyl groups is a challenging issue. Primary hydroxyl groups, such as the C-5–C-6–O-6–HO-6 moiety in hexopyranoses (Fig. 1), show an interesting conformational behaviour, which was inaccurately modelled by early generations of carbohydrate force fields. Experimental crystal structures of carbohydrate–protein complexes and carbohydrates showed that the C-5–C-6 bond can exist in three canonical conformers, namely in *gauche–gauche* (*gg*), *gauche–trans* (*gt*) and *trans–gauche* (*tg*). Populations of individual rotamers in solution can be estimated using NMR spectroscopy from measured homonuclear ($^3J_{\text{H-5–H-6}}$) or heteronuclear ($^3J_{\text{C-4-H-6}}$) vicinal coupling constants. For methyl α-D-glucopyranoside, the experimentally predicted percentage populations for *gt*, *tg* and *gg* rotamers are 38%, 5% and 57%, respectively.[7] For methyl α-D-galactopyranoside the corresponding populations are 47%, 39% and 14%.[7]

Potential energies of these rotamers can be calculated for static structures in vacuum using molecular mechanics, ab initio, or density functional theory (DFT) methods.[8,9] However, their energetics in vacuum and at 0 K is poorly related to the situation in solvent and at biologically relevant temperatures, even if a high level of theory is used. For example, the *trans–gauche* (*tg*) conformation of methyl α-D-glucopyranoside was predicted to be energetically favourable in vacuum, when, in fact, it was almost absent in a water environment. In order to realistically model populations of C-5–C-6 rotamers it was necessary to include the effect of solvent.

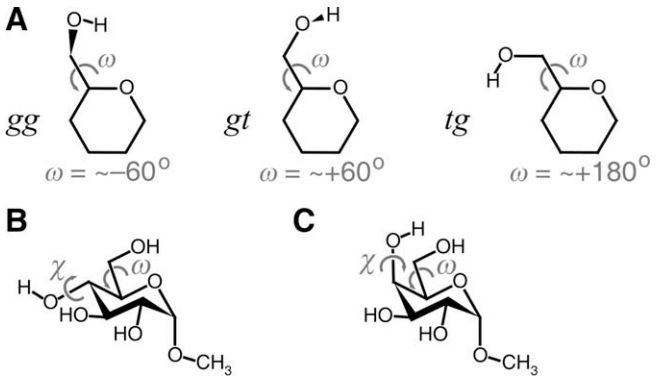

Figure 1. (A) Schematic representation of *gauche–trans* (*gt*), *trans–gauche* (*tg*) and *gauche–gauche* (*gg*) conformations, (B) methyl α-D-glucopuranoside (α-D-Glc*p*-OMe, **1**), (C) methyl α-D-galactopyranoside (α-D-Gal*p*-OMe, **2**).

In the context of hexopyranoses, the propensity of ω torsional angle (O-5–C-5–C-6–O-6) to adopt the *gauche* conformation is often being explained by the *gauche* effect,[10] that is, the rotamers with two oxygens in *gauche* orientation tend to be more stable. However, this effect can be compensated by hydrogen bonding between O-6–HO-6 and O-4–HO-4 moieties. Both these phenomena, the *gauche* effect and hydrogen bonding, can be accurately addressed by DFT and ab initio techniques in the gas phase[8,9] and in the development of empirical force fields. However, the situation becomes more complicated when a solvent comes into play. The first attempt in finding a solution to the problem of solvent effects was the application of an implicit solvation model. Energies calculated at the DFT level of theory, together with the self-consistent interaction field solvent model, were in sound agreement with experimental populations.[8]

Alternatively, it is possible to perform a very long molecular dynamics simulation in an explicitly modelled solvent. The resulting trajectory can be analysed to calculate populations of individual rotamers. This approach was applied by Kirschner and Woods.[11] In a 50-ns MD simulation of methyl α-D-glucopyranoside, they observed 15 transitions between *gauche–trans*, *trans–gauche* and *gauche–gauche* conformations. By analysis of the resulting trajectory they found that the *gauche–gauche* conformation was the most populated (54%), followed by *gauche–trans* (40%), and the *trans–gauche* conformation was least populated (6%), all in good agreement with experimental results. A correlative simulation for methyl α-D-galactopyranoside led to *gt*, *tg* and *gg* rotamer populations of 64%, 28% and 8%, respectively.

In this study we apply the metadynamics method to simulate rotamer equilibria of a primary hydroxyl group (Fig. 1) in methyl α-D-glucopyranoside (α-D-Glc*p*-OMe, **1**) and methyl α-D-galactopyranoside (α-D-Gal*p*-OMe, **2**) in vacuum and an explicit water environment. The free-energy surface for **1** and **2** was calculated as a function of two variables. The first collective variable was the ω torsional angle (O-5–C-5–C-6–O-6). The χ torsional angle (C-3–C-4–O-4–HO-4) was chosen as the second collective variable because it controls clockwise versus counter-clockwise orientations of secondary hydroxyl groups that are especially important in vacuum.

2. Models and methods

Metadynamics calculates the free-energy surface in the space of a few (typically two) parameters (collective variables), and their choice is the first step in the application of metadynamics. In order to quantitatively study torsional equilibrium of primary hydroxyl rotamers, it was essential to choose the torsional angle ω (O-5–C-5–C-6–O-6, Fig. 1) as the first collective variable. It is useful to use a bias potential that improves sampling of all potentially slow degrees of freedom within the system. Important degrees of freedom that are not biased by the metadynamics potential may cause poor convergence and hysteresis in calculated free-energy surfaces. The second important degree of freedom of the studied system is rotation of the secondary hydroxyl groups. Especially in vacuum, these hydroxyl groups form a hydrogen-bond network with either a clockwise (*c*) or a counter-clockwise (*cc*) orientation. These orientations influence the populations of primary hydroxyl rotamers. Therefore, the torsional angle χ (C-3–C-4–O-4–HO-4) was selected as the second collective variable.

The duration of each metadynamics run was initially set to 10 ns. However, after approximately 8 ns of the metadynamics run of α-D-Glc*p*-OMe (**1**) in water, the molecule started to explore

ring conformations other than $^4C_1$. Because these conformations (boat, skew-boat and $^1C_4$) are relatively rare in glucose equilibrium, we decided to exclude this part of the metadynamics run and analyse only 5 ns of each simulation.

All metadynamics simulations were performed in GROMETA 2.0—a metadynamics addendum[12] to GROMACS.[13] GLYCAM06 force field topology was obtained from the GLYCAM web site[14] and converted to the GROMACS format using a modified *amb2gmx.pl* script.[15] It was necessary to modify the script because the original script ignores torsional terms with negative force constants. Converted topology was tested by comparing potentials calculated using GROMACS and AMBER[16] software. Both electrostatic and van der Waals 1–4 interactions were not scaled, contrary to usual formalism of AMBER force fields. This was reported to be necessary for accurate modelling of rotamer equilibrium of primary hydroxyl groups in carbohydrates.[11]

In vacuum the system was simulated using Langevin dynamics with a 1-fs step and without any constraints. Electrostatic interactions were modelled using a single cutoff set to 1.6 nm. After energy minimisation, the system was pre-equilibrated by a 0.2 ns MD simulation. Temperature was kept constant at 300 K using a Berendsen thermostat.[17] In water simulations, the system was placed in a box ($3 \times 3 \times 3$ nm) containing one molecule of solute and 884 TIP3P water molecules.[18] The system was simulated using Newtonian dynamics with a 1-fs step and no constraints applied to the solute. Electrostatic interactions were modelled using a particle-mesh Ewald method[19] with the cutoff set to 1.0 nm. After energy minimisation, the system was pre-equilibrated by a 200-fs simulation in the NPT ensemble, followed by 200 ps in the NVT ensemble. The temperature was kept constant at 300 K using a Berendsen thermostat.[17]

Metadynamics simulations in vacuum, and then in water, were performed by running a 5 ns MD simulation at 300 K, during which a bias potential accumulated. At every 1 ps, a Gaussian hill of height $w = 0.1$ kJ/mol and width $\delta s = 0.3$ radian was added. Error bars were calculated at the level of 95% probability.

3. Results and discussion

Assuming two dihedral angles ω and χ as conformational variables, both studied molecules can, in principle, adopt three primary hydroxyl orientations (*gt*, *tg* and *gg*) and three secondary hydroxyl orientations (approx. −60°, +60° and 180°), giving a total of nine possible combinations. Not all of these combinations correspond to stable conformations predicted by metadynamics. As already mentioned, studied the molecules studies in vacuum showed high cooperativity of hydroxyl groups as a result of hydrogen bonding. These groups are oriented either clockwise or counter-clockwise. This cooperativity is supported by experimental R2PI (resonant 2-photon ionisation) and IR ion dip spectra of monosaccharides measured under conditions of supersonic jet expansion.[20–24] Thanks to this cooperativity, it is possible to improve the sampling of clockwise versus counter-clockwise equilibrium by biasing only the single dihedral angle χ (C-3–C-4–O-4–HO-4).

It turned out that one molecule had sampled conformations other than $^4C_1$, and it was therefore necessary to reduce the length of each metadynamics run. The GLYCAM06 force field[14] has been developed and evaluated to accurately model ring puckering of monosaccharides. A conformational transition of the α-D-Glc*p*-OMe molecule to conformations other than $^4C_1$ is not very probable within a 10-ns time scale. The fact that such a transition was observed can be explained by a complementary effect of the bias potential, that is, it can increase fluctuations to this degree of freedom. Alternatively, it could be proposed that the absence of 1–4 scaling, which is crucial for accurate modelling of rotamer equilibria, makes modelling of ring-puckering transitions less accurate. This should be included in future research.

Figure 2 shows the two-dimensional (ω, χ) free-energy surfaces of **1** and **2** in vacuum and in water. Minimum, with the ω values of ∼−60°, ∼+60° and ∼180°, corresponds to the *gg*, *gt* and *tg* conformations, respectively. In the free-energy surface of α-D-Glc*p*-OMe (**1**, Fig. 2A), the χ values of ∼180° and ∼+60° correspond to the clockwise and counter-clockwise orientations of the hydrogen bonding network. The (ω, χ) free-energy surface shows four major free-energy minima (**a**–**d**) with similar values of free energy, namely *cc-gg*, *cc-gt*, *cc-tg* and *c-tg*. Corresponding molecular structures are depicted in the top row of Figure 3. Similarly, conformations in water discussed later are depicted in Figure 4. These conformations (10 for each minimum) were selected from the metadynamics pseudo-trajectory as conformations with values of collective variables closest to a given free-energy minimum. Structures of minima **a**–**d** show that orientations of secondary hydroxyl groups are almost purely clockwise or counter-clockwise. Moreover, orientation of the primary hydroxyl group is the same within each minimum, even if this group is not involved in a hydrogen bond.

Two-dimensional free energy surfaces shown in Figure 2 can be integrated into a one-dimensional free energy surface (Fig. 5) using the equation:

$$A(\omega) = \frac{1}{\beta} \ln \left[\int_{-\pi}^{\pi} e^{-\beta A(\chi,\omega)} d\chi \right] \quad (2)$$

where A is free energy and β is inverse temperature ($1/k_BT$). A global free-energy minimum of each one-dimensional free-energy surface was taken as zero. The accuracy was calculated by evaluating free-energy convergence between 2500 and 5000 steps of metadynamics. The resulting one-dimensional free-energy surface of **1** in vacuum (Fig. 5A) shows that the *tg* conformation is slightly more favourable. This can be explained by the fact that the OH-6 group can act as a hydrogen bond acceptor as well as a hydrogen bond donor in the *tg* conformation (minima **c** and **d**). These interactions correspond to the clockwise and counter-clockwise orientations of hydroxyl groups and contribute to a stability of the *tg* conformation. On the other hand, in the *gg* (**a**) and *gt* (**b**) rotamers, the orientation of hydroxyls is almost purely counter-clockwise because this kind of hydrogen bond network is more stable when the OH-6 group does not participate. The fact that the *tg* conformation is present in vacuum is in agreement with experimental data on phenyl β-D-glucopyranoside; however, the *c-tg* (**d**) conformation has not been experimentally detected.[20,21]

In water, α-D-Glc*p*-OMe (**1**) shows much lower free-energy barriers and loose cooperativity in the secondary hydroxyl groups (Fig. 2B). This is illustrated by structures depicted in Figure 4 (**e**–**j**). The most remarkable is a loss of cooperativity between secondary hydroxyl groups, which adopt different orientations, contrary to the situation in vacuum. This explains the fact that stability of structures with the χ angle of ∼−60° became comparable to those with χ values of +60°. Similarly, also the primary hydroxyl group adopts different orientations of the OH-6 group within each minimum. To further illustrate the role of water, Figure 4 shows that the oxygen atoms of water molecules are closer than 3 Å to the atom O-6. These water molecules are located in positions suitable for hydrogen bonding between the primary hydroxyl group and a water molecule. In some minima, it seems that water molecules cluster in a particular position (e.g., close to O-5 in the minimum **f**). We assume that the conformational preference of the C-5–C-6–O-6–HO-6 moiety is responsible for this arrangement, rather than a formation of a hydrogen-bonding network. There was no evidence for the existence of a water molecule steadily bound to two different sites of glucopyranose.

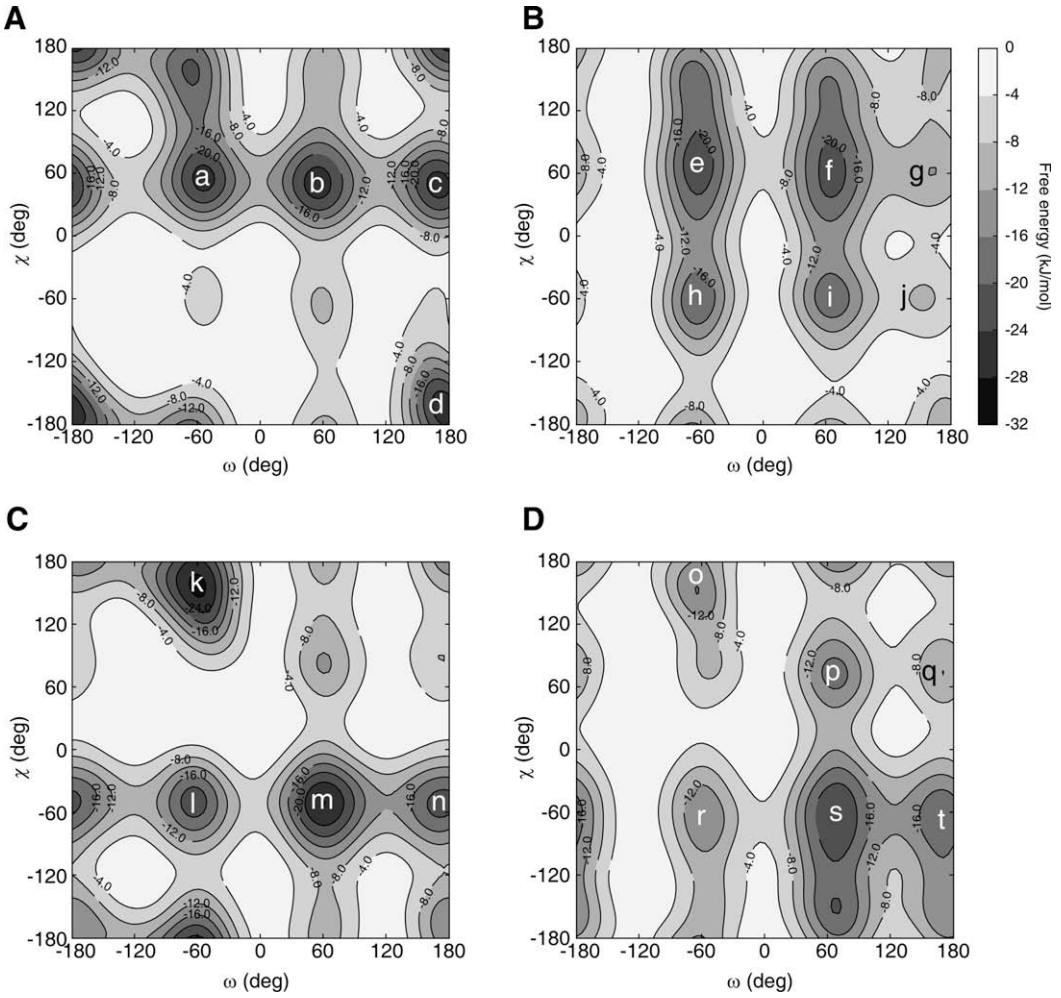

Figure 2. Results of metadynamics—the two-dimensional free-energy surface of α-D-Glc*p*-OMe (**1**) in vacuum (A) and in water (B) and α-D-Gal*p*-OMe (**2**) in vacuum (C) and in water (D). Selected free-energy minima (**a**–**t**) are depicted in Figures 3 and 4.

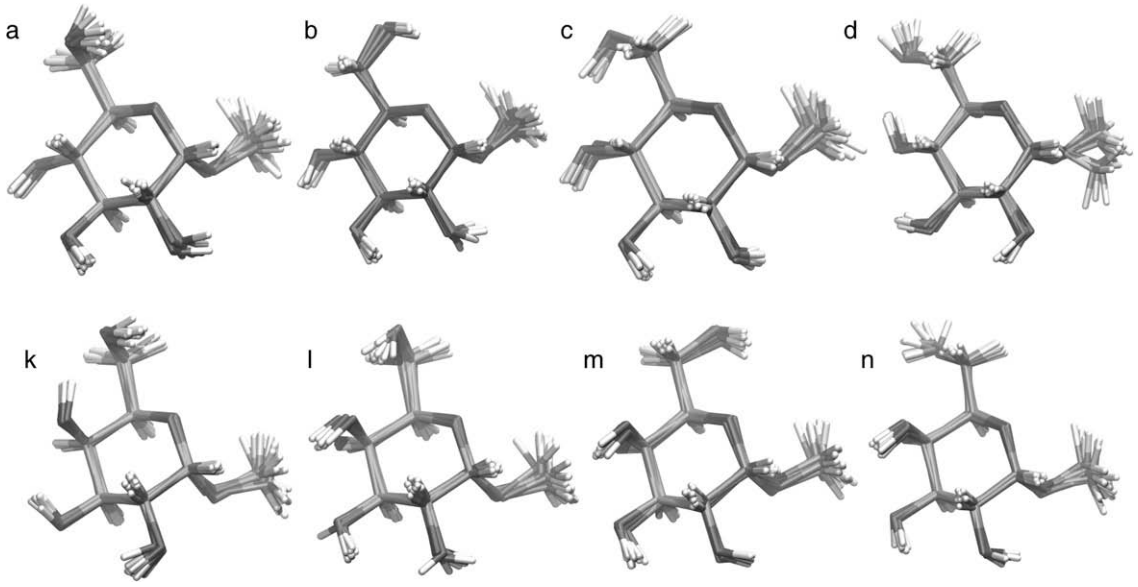

Figure 3. Conformations corresponding to free-energy minima of **1** (minima **a**–**d** from Fig. 2A) and **2** in vacuum (minima **k**–**n**. from Fig. 2C). Ten snapshots from a metadynamics pseudo-trajectory with values of collective variables closest to the minimum were superimposed for each minimum.

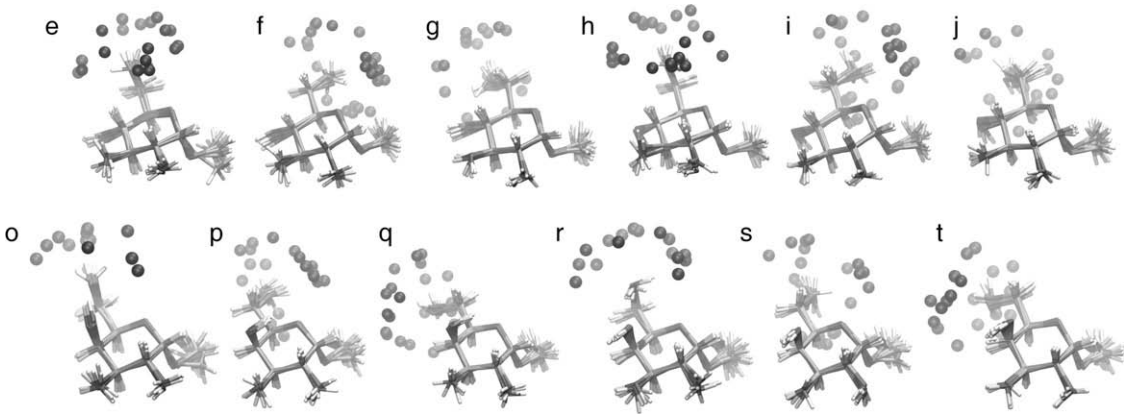

Figure 4. Conformations corresponding to the free-energy minima of **1** in water (minima **e**–**j** from Fig. 2B) and **2** in water (minima **o**–**t**. from Fig. 2D). Ten snapshots for each minimum from a metadynamics pseudo-trajectory were superimposed as in Figure 3. Oxygen atoms from water molecules closer than 3 Å to the O-6 atom are shown as spheres.

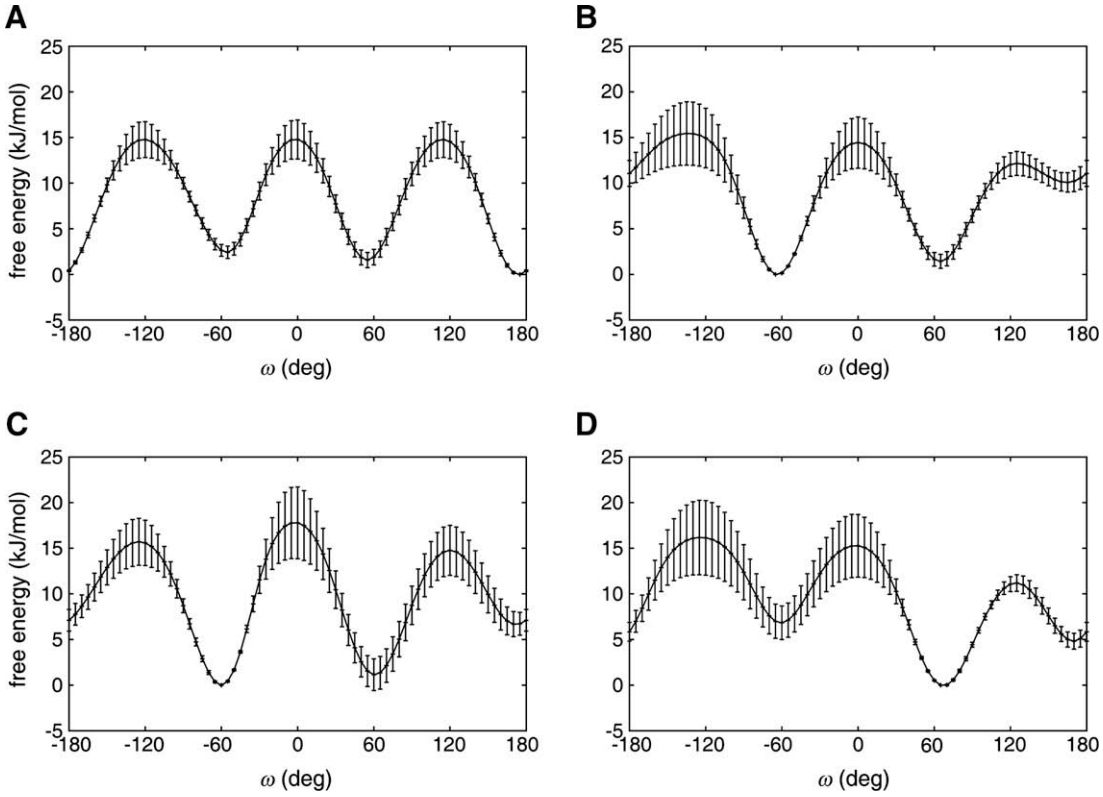

Figure 5. One-dimensional free-energy surfaces obtained by integration of two-dimensional surfaces in Figure 2. Free-energy surfaces for α-D-Glc*p*-OMe (**1**) in vacuum (A) and in water (B) and for α-D-Gal*p*-OMe (**2**) in vacuum (C) and in water (D).

The water environment significantly influences the rotamer equilibrium of secondary hydroxyl groups by equalising free energies of conformers with angle χ of $\sim$+60° and −60°. On the contrary, the *tg* conformations that are preferred in vacuum are destabilised by solvent effects and are the least populated rotamers in water. The one-dimensional free energy surface (Fig. 5B) further demonstrates this fact.

The (ω, χ) free energy surface of α-D-Gal*p*-OMe (**2**) in vacuum (Fig. 2C) is significantly different from the free-energy surface of **1**. However, it does resemble the free-energy surface of **1** in vacuum rotated by 180° around the point with $\omega = \sim$60° and $\chi = \sim$0°. Minimum **n** corresponds to the minimum **a** (both are without hydrogen bonding between OH-6 and OH-4 groups); minimum **m** corresponds to **b** (OH-6 is aligned to O-5 in both molecules). Equally, minimum **l** corresponds to **c** and **k** corresponds to **d.** All these four conformers contain a hydrogen bond between OH-6 and OH-4 groups, but their functioning as a donor or acceptor is replaced. Due to an axial orientation of the C4 hydroxyl group, the OH-6 group can act as the hydrogen-bond donor or acceptor in the *gg* (**k** and **l**) conformations. Therefore, the *gg* conformation, similar to the *tg* rotamer in **1**, can be involved in both a clockwise or counter-clockwise hydrogen-bonding network. Similarly to **1**, hydrogen bonding is also cooperative and **2** shows either clockwise or counter-clockwise orientation of hydroxyl groups. Only one of 10 snapshots in the minimum **l** showed a different orientation of hydroxyl groups than in other snapshots. Also orientation of the

primary hydroxyl group was the same within each minimum with the largest variability observed for the minimum **n**. Gas phase spectra of phenyl β-D-galactopyranoside[21] support three of four structures predicted by metadynamics, namely *c-gg* (**k**), *cc-gt* (**m**) and *cc-tg* (**n**).

It appears that solvent effects influence the calculated free-energy surface of α-D-Gal*p*-OMe **2** in a similar way as in the case of **1,** by lowering free energy barriers on angle χ. The most significant difference is a decreased stability of the *gg* conformation (**k**. and **l**. vs **o**. and **r**.) in water compared to vacuum (Fig. 2D). As a result, the *gt* conformation is the most favourable conformation in water, as demonstrated by the one-dimensional free energy surface shown in Figure 5D.

Rotamer compositions (x_i) were calculated from free energy values in order to compare the results of metadynamics simulations with experimental data.[7,8,25–27] The free-energy value A_i of each minimum was converted to probability $\exp(-\beta A_i)$. Accuracy (i.e., confidence intervals) was evaluated by the calculation of minimal and maximal populations of each rotamer. For example, to obtain the minimal population of a selected *i*th rotamer, the probability was calculated from its free energy + error. Then, probabilities of two other rotamers were calculated from their free energy − error. Finally, the composition was calculated as $x_i = \exp(-\beta A_i)/\Sigma\exp(-\beta A_j)$. Similarly, maximal populations were calculated by subtracting and adding an error value to the free energy of rotamers. Results with confidence intervals are depicted in Figure 6 as dark bars. In addition, experimental estimates from homonuclear[7,8,25–27] and heteronuclear[8] couplings are included in Figure 6.

Accuracy of the modelled free-energy surfaces can be evaluated by comparison of experimental NMR coupling constants with values predicted using Karplus-type equations. The metadynamics bias potential acts on the ω dihedral angle and not directly on experimentally estimated dihedrals C-4–C-5–C-6-$H^{R/S}$-6 or H-5–C-5-C-6-$H^{R/S}$-6. However, these dihedral angles are strongly correlated with the collective variable ω because they are all C-5–C-6 dihedrals. Relationships between these angles and ω were fitted with a polynomial of degree of four. These polynomials were then used to calculate probabilities of C-4–C-5–C-6-$H^{R/S}$-6 or H-5–C-5-C-6-$H^{R/S}$-6 dihedral angles from the calculated free-energy surface.

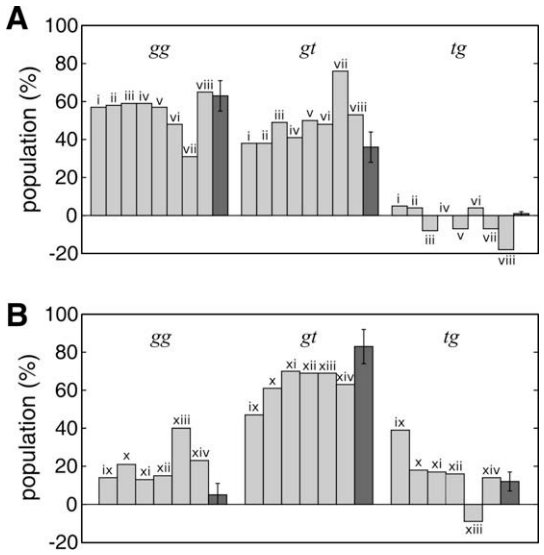

Figure 6. Comparison of the experimental rotamer populations (grey bars) and the calculated populations from metadynamics simulations (dark bars) in water for α-D-Glc*p*-OMe (A) and α-D-Gal*p*-OMe (B). Experimental data were determined from $^3J_{H\text{-}5\text{–}H\text{-}6}$ (i and ix,[7] ii–iv and x–xi,[25] v,[26] vi,[27] vii and xiii[8]) and $^3J_{C\text{-}4\text{–}H\text{-}6}$ coupling measurements (viii and xiv[8]).

Table 1
Comparison of the calculated vicinal $^3J_{C\text{-}4\text{–}H\text{-}6}$ and $^3J_{H\text{-}5\text{–}H\text{-}6}$ coupling constants (Hz) with NMR experimental values[8]

Compound		$^3J_{C\text{-}4\text{–}H\text{-}6R}$	$^3J_{C\text{-}4\text{–}H\text{-}6S}$	$^3J_{H\text{-}5\text{–}H\text{-}6R}$	$^3J_{H\text{-}5\text{–}H\text{-}6S}$
α-D-Glc*p*-OMe (**1**)	Calcd	1.3	5.2	5.5	3.5
	Obsd.	1.1	2.9	5.4	2.2
α-D-Gal*p*-OMe (**2**)	Calcd	1.8	2.2	8.8	3.1
	Obsd.	0.9	3.7	8.3	4.0

The average values of coupling constants were finally calculated (Eq. 2) by integration of dihedral probability multiplied by a corresponding coupling constant, calculated using Karplus-type equation for vicinal carbon–proton[28] (Eq. 3) or proton–proton couplings[29] (Eq. 4), respectively:

$$^3J = \frac{\int_{-\pi}^{\pi} {}^3J(\phi)\exp(-\beta A(\phi))d\phi}{\int_{-\pi}^{\pi}\exp(-\beta A(\phi))d\phi} \quad (3)$$

$$^3J_{C\text{-}4\text{–}H\text{-}6} = 5.8\cos^2(\phi) - 1.6\cos(\phi) + 0.28\sin(2\phi) - 0.02\sin(\phi) + 0.52 \quad (4)$$

$$^3J_{H\text{-}5\text{–}H\text{-}6} = 13.22\cos^2(\phi) - 0.99\cos(\phi) + \sum \Delta\chi_i^{ele}\left\{0.87 - 2.46\cos^2\left(\xi_i\phi + 0.347\left|\Delta\chi_i^{ele}\right|\right)\right\} \quad (5)$$

where χ^{ele} is electronegativity and ξ is +1 or −1, depending on the orientation of substituents. The resulting coupling constants are presented in Table 1 in comparison with experimental values. Homonuclear coupling constants were in good agreement with experimentally observed values, with the $^3J_{H\text{-}5\text{–}H\text{-}6S}$ showing larger differences. However, it appears that the calculated $^3J_{C,H}$ couplings exhibit a larger discrepancy with experimental values. It can be seen in Table 1 that the larger differences between the experimental and calculated values are found for $^3J_{C\text{-}4\text{–}H\text{-}6S}$ constants. This can be explained by a lower accuracy of measured heteronuclear coupling constants on one side and by a large sensitivity of the used conformational dependence of $^3J_{C,H}$ couplings on torsion angle (Eq. 3). It is noteworthy that larger discrepancies are associated with the H-6^S atom. We observed a similar behaviour in our previous paper.[8]

The major effect of a water environment is the reduction of the *tg* rotamer population in **1** and the *gg* rotamer population in **2**. This is in agreement with other studies of this system.[8,11] By comparing two-dimensional free-energy surfaces (Fig. 2) it can be explained that this reduction is caused by the fact that conformations with a hydrogen bond between OH-4 and OH-6 hydroxyl groups, which are favourable in vacuum (**c**, **d**, **k** and **l**), are disfavoured in a water environment (**g**, **o** and **r**). Recently, it has been experimentally observed that singly hydrated monosaccharides show drastically different conformational preferences compared to bare molecules.[21,22,24]

Free-energy modelling techniques, such as umbrella sampling or metadynamics, can achieve relatively high accuracy in terms of free-energy convergence. Here we achieved an accuracy of better than 2 kJ/mol and better than 10% in populations. Resulting populations of both molecules are in good agreement with a long unbiased simulation, as well as the experimental data from homonuclear coupling measurements. Results of this study demonstrate good accuracy of the GLYCAM06 potential in modelling rotamer equilibria. As far as we are aware, modelling of conformational preferences of carbohydrate primary hydroxyl groups is a rare case where accurate experimental data, as well as accurate and computationally effective potential, are both available. The results of metadynamics simulations are in good agreement with long unbiased molecular dynamics simulations and with experiment, and

together with recent investigation of ring conformations of pyranoses,[4,30] they show that metadynamics can be applied to conformational problems not easily described by conventional modelling methods. This also supports the theoretical background of metadynamics that the use of a bias potential approximates the free energy surface of the studied system described by selected degrees of freedom.[31,32]

4. Conclusions

In this study we obtained one- and two-dimensional conformational free-energy surfaces of two methyl hexopyranosides in vacuum and in water. Whereas two-dimensional (ω, χ) free-energy surfaces help to reveal hydrogen-bonding networks and their equilibrium, the one-dimensional (ω) free-energy surfaces provide a comparison between theory and experiment. It was observed that a water environment significantly changes conformational equilibrium in methyl hexopyranosides, mostly by a disruption of hydrogen bonds between the C-4 and C-6 hydroxyl groups.

Acknowledgements

This investigation was supported by grants from the Science and Technology Assistance Agency under Contract APVV-0607-07 and from the Centres of Excellence programme of the Slovak Academy of Sciences (COMCHEM, Contract No. II/1/2007). V.S. would like to acknowledge support from the Czech Ministry of Education, Youth and Sports (MSM6046137305).

References

1. In *NMR Spectroscopy and Computer Modelling of Carbohydrates*; Vliegenthart, J. F. G.; Woods, R. J., Eds.; ACS Symposium Series, 2006; Vol. 930, pp 285–301.
2. Laio, A.; Parrinello, M. *Proc. Natl. Acad. Sci. U.S.A.* **2002**, *99*, 12562–12566.
3. Laio, A.; Gervasio, F. L. *Rep. Prog. Phys.* **2008**, *71*, 126601.
4. Biarnés, X.; Ardevol, A.; Planas, A.; Rovira, C.; Laio, A.; Parrinello, M. *J. Am. Chem. Soc.* **2007**, *129*, 10686–10693.
5. Ensing, B.; Klein, M. L. *Proc. Natl. Acad. Sci. U.S.A.* **2005**, *102*, 6755–6759.
6. Quigley, D.; Rodger, P. M. *J. Chem. Phys.* **2008**, *128*, 154518.
7. Nishida, Y.; Ohrui, H.; Meguro, H. *Tetrahedron Lett.* **1984**, *25*, 1575–1578.
8. Tvaroška, I.; Taravel, F. R.; Utille, J. P.; Carver, J. P. *Carbohydr. Res.* **2002**, *337*, 353–367.
9. Tvaroška, I.; Carver, J. P. *J. Phys. Chem. B* **1997**, *101*, 2992–2999.
10. Wolfe, S. *Acc. Chem. Res.* **1972**, *5*, 102–111.
11. Kirschner, K. N.; Woods, R. J. *Proc. Natl. Acad. Sci. U.S.A.* **2001**, *98*, 10541–10545.
12. Bonomi, M.; Gervasio, F. L.; Tiana, G.; Provasi, D.; Broglia, R. A.; Parrinello, M. *Biophys. J.* **2007**, *93*, 2813–2821.
13. van der Spoel, D.; Lindahl, E.; Hess, B.; Groenhof, G.; Mark, A. E.; Berendsen, H. J. *J. Comput. Chem.* **2005**, *26*, 1701–1718.
14. Kirschner, K. N.; Yongye, A. B.; Tschampel, S. M.; González-Outeiriño, J.; Daniels, C. R.; Foley, B. L.; Woods, R. J. *J. Comput. Chem.* **2008**, *29*, 622–655.
15. http://chemistry.csulb.edu/ffamber/tools.html, September 2008.
16. Case, D. A.; Cheatham, T. E., III; Darden, T.; Gohlke, H.; Luo, R.; Merz, K. M., Jr.; Onufriev, A.; Simmerling, C.; Wang, B.; Woods, R. J. *J. Comput. Chem.* **2005**, *26*, 1668–1688.
17. Berendsen, H. J. C.; Postma, J. P. M.; DiNola, A.; Haak, J. R. *J. Chem. Phys.* **1984**, *81*, 3684–3690.
18. Berendsen, H. J. C.; Postma, J. P. M.; van Gunsteren, W.; Hermans, J. Interaction models for water in relation to protein hydration. In *Intermolecular Forces*; Pullman, B., Ed.; Reidel: Dordrecht, 1981; pp 331–342.
19. Essmann, U.; Perera, L.; Berkowitz, M. L.; Darden, T.; Lee, H.; Pedersen, L. G. *J. Chem. Phys.* **1995**, *103*, 8577–8592.
20. Talbot, F. O.; Simons, J. P. *Phys. Chem. Chem. Phys.* **2002**, *4*, 3562–3565.
21. Çarçabal, P.; Jockusch, R. A.; Hünig, I.; Snoek, L. C.; Kroemer, R. T.; Davis, B. G.; Gamblin, D. P.; Compagnon, I.; Oomens, J.; Simons, J. P. *J. Am. Chem. Soc.* **2005**, *127*, 11414–11425.
22. Cocinero, E. J.; Stanca-Kaposta, E. C.; Scanlan, E. M.; Gamblin, D. P.; Davis, B. G.; Simons, J. P. *Chem. Eur. J.* **2008**, *14*, 8947–8955.
23. Screen, J.; Stanca-Kaposta, E. C.; Gamblin, D. P.; Liu, B.; Macleod, N. A.; Snoek, L. C.; Davis, B. G.; Simons, J. P. *Angew. Chem., Int. Ed.* **2007**, *46*, 3644–3648.
24. Stanca-Kaposta, E. C.; Gamblin, D. P.; Screen, J.; Liu, B.; Snoek, L. C.; Davis, B. G.; Simons, J. P. *Phys. Chem. Chem. Phys.* **2007**, *9*, 4444–4451.
25. Bock, K.; Duus, J. O. *J. Carbohydr. Chem.* **1994**, *13*, 513–543.
26. Rockwell, G. D.; Grindley, T. B. *J. Am. Chem. Soc.* **1998**, *120*, 10953–10963.
27. Nishida, Y.; Hori, H.; Ohrui, H.; Meguro, H. *J. Carbohydr. Chem.* **1988**, *7*, 239–250.
28. Tvaroška, I.; Gajdoš, J. *Carbohydr. Res.* **1995**, *271*, 115–162.
29. Haasnoot, C. A. G.; de Leeuw, F. A. A. M.; Altona, C. *Tetrahedron* **1980**, *36*, 2783–2792.
30. Spiwok, V.; Tvaroška, I. *J. Phys. Chem. B*, 113, in press.
31. Laio, A.; Rodriguez-Fortea, A.; Gervasio, F. L.; Ceccarelli, M.; Parrinello, M. *J. Phys. Chem. B* **2005**, *109*, 6714–6721.
32. Bussi, G.; Laio, A.; Parrinello, M. *Phys. Rev. Lett.* **2006**, *96*, 090601.